Appl. Phys. A 81, 1345–1349 (2005)
DOI: 10.1007/s00339-005-3321-2

**Applied Physics A**
**Materials Science & Processing**

G.S. HUANG[1]
X.L. WU[1,✉]
L.W. YANG[1]
X.F. SHAO[1]
G.G. SIU[2]
P.K. CHU[2]

# Dependence of blue-emitting property on nanopore geometrical structure in Al-based porous anodic alumina membranes

[1] National Laboratory of Solid State Microstructures and Department of Physics, Nanjing University, Nanjing 210093, P.R. China
[2] Department of Physics and Materials Science, City University of Hong Kong, Kowloon, Hong Kong, P.R. China

**Received: 7 May 2005/Accepted: 22 June 2005**
**Published online: 4 August 2005 •** 

**ABSTRACT** Porous anodic alumina (PAA) membranes were fabricated using anodization of Al foils. Based on morphology observations and photoluminescence (PL) measurements, it is revealed that the peak position of the observed blue PL band has an evident dependence on nanopore geometrical structure. The blue PL band is asymmetrical and can be Gaussian divided into two subbands, which originate in two kinds of oxygen-deficient centers, $F^+$ and $F$ centers. On raising the anodic voltage, the two subbands red shift and the intensity of the subband from the $F^+$ centers relative to that from the $F$ centers increases. This suggests that the increases of nanopore size and porosity make partial $F^+$ centers convert into $F$ centers. The mechanism of this conversion is further discussed on the basis of the PL behavior of the PAA membrane under ultraviolet irradiation. This work will be beneficial to the better understanding of the PL property of the PAA membrane.

**PACS** 78.55.-m; 82.45.Cc; 76.30.Mi

In recent years, a porous anodic alumina (PAA) membrane with an ordered nanopore array has attracted an increasing interest, because of its favorable applications as a template in fabricating nanostructured materials [1–9], such as carbon nanotubes (CNTs) [10], Ni nanotubules [11], Si nanodots [12], CdS nanoparticles [13], ZnO nanowire arrays [14], and $Eu_2O_3$ nanotube arrays [15]. Of all the fabricated materials, their light-emitting properties have become a subject of many experimental and theoretical investigations due to the applications in optoelectronics [14, 15]. However, it is well known that the PAA membrane itself has a strong blue photoluminescence (PL). Therefore, when we use the template to fabricate some nanomaterials with light-emitting properties, a difficulty rises: how should we identify the light emission of the template itself from the obtained radiation [1]? Due to this difficulty, over the past years many investigators have drawn attention to the light-emitting properties of the PAA membrane. Some models have been presented to describe the PL mechanism. Du et al. [16] and Li et al. [17] attributed the blue PL to optical transitions in individual $F^+$ centers. Gao et al. [18] suggested that the blue PL originates in oxalic impurities. Li et al. [19] correlated the blue PL with oxygen-related centers and aluminum incorporated into the anion-contaminated alumina layer. Since the microscopic details are complicated, the existing data and explanations are unclear or still controversial. More work is needed to further reveal the blue-emitting property and clarify its mechanism. Recently, we noted that the blue-emitting property has an evident dependence on nanopore geometrical structure of the PAA membrane. This dependence contains important and significant information in understanding the PL property and thus deserves to be studied deeply.

In this work, we firstly fabricate the PAA membranes with different nanopore sizes and porosities and then investigate their PL properties. In view of the obvious asymmetry of the obtained PL spectra, we Gaussian divide each spectrum into two PL bands with their origins in the $F^+$ and $F$ centers [20]. We found that on raising the anodic voltage, the intensity of the subband from the $F^+$ centers relative to that from the $F$ centers increases, which indicates that partial $F^+$ centers have transformed into the $F$ centers. We further discuss the mechanism of this conversion on the basis of the PL behavior of the PAA membrane under ultraviolet irradiation.

High-purity Al foils (99.99%) were used to fabricate the PAA membranes. The Al foil was firstly electropolished in a mixed solution of perchloric acid and ethanol (1 : 5 by volume) under a constant dc voltage of 18 V for 3 min. Anodization with a platinum plate as a cathode and the Al foil as an anode was conducted in 0.5 M oxalic acid under different dc voltages of 20, 30, 40, 50, and 60 V. The electrolyte was maintained at 5 °C by placing the electrolytic bath in a refrigerator and it was mechanically stirred. A two-step anodic process was adopted to obtain a high-quality PAA membrane [21]. The Al foil was firstly anodized for 1 h as the first step, followed by immersion into a mixture of 5 wt. % phosphoric acid and 1.8 wt. % chromic acid (1 : 1 by volume) at 75 °C for 2 h to remove the alumina layer grown in the first step. The second step adopts the same experimental conditions, but the anodization lasts for 2 h to obtain a thick PAA membrane with light emission. During the anodization, the current–time ($I$–$t$) curves were recorded to monitor the growth process and compare the influence of different applied anodic voltages on the geometrical structure of the PAA membrane. In our experiments, the surface morphologies of the PAA membranes were characterized using a LEO 1530VP field emission scan-

✉ Fax: 86-25-83595535, E-mail: hkxlwu@nju.edu.cn

ning electron microscope (SEM). PL spectra were taken on a FluoroMax-2 fluorescence spectrophotometer (Jobin-Yvon Co.) with a 150-W Xe lamp as excitation source. During PL measurements, the slit width was set at 5 mm and each spectrum was rapidly acquired within less than 2 min. All the measurements were carried out at room temperature.

Figure 1 shows a series of SEM images of the PAA membranes formed in 0.5 M oxalic acid under different anodic voltages. Though local hexagonal arrangements of the nanopores can be observed in all the membranes, a highly ordered nanopore array only exists in the membranes formed under 40 and 50 V. This result indicates that perfect self-organized growth, which controls the nanopore arrangement, only occurs under a certain anodic voltage. This is 40 or 50 V in our present experiments. From these SEM images, one can also see that both nanopore diameter $d_p$ and interpore distance $d_c$ increase with the anodic voltage. The corresponding results are shown in Fig. 2. A linear dependence of $d_c$ on the applied voltage is pronounced [5, 22, 23]. Previously, a similar phenomenon was observed and described using a simple formula [24]:

$$R_m = kU_a, \tag{1}$$

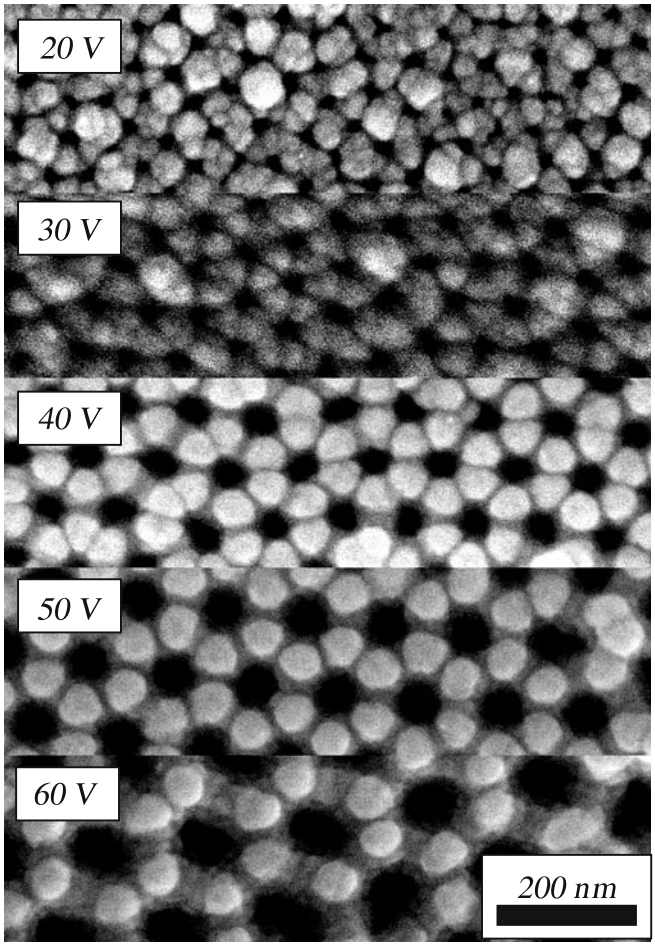


**FIGURE 1** A series of SEM images of the PAA membranes formed using anodization of Al foil in 0.5 M oxalic acid under different constant dc voltages of 20, 30, 40, 50, and 60 V, respectively

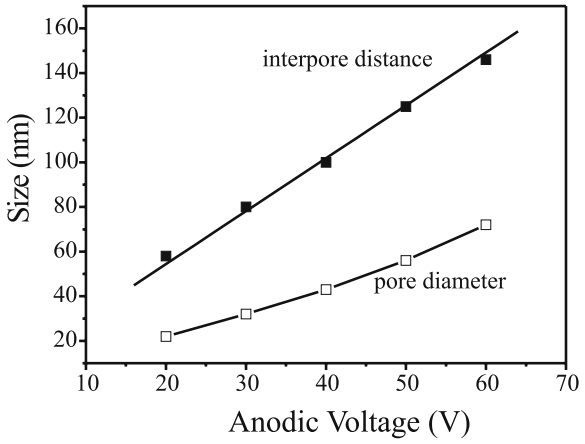


**FIGURE 2** Average interpore distance and pore diameter as a function of the applied anodic voltage

where $R_m$ is the interpore distance and $U_a$ the applied anodic voltage. $k$ is a constant. In a previous investigation [24], it was found that the above formula is also suitable for the dependence of $d_p$ on the applied voltage. However, our present experiment shows a nonlinear dependence of $d_p$ on the anodic voltage. $d_p$ becomes larger under high anodic voltage. This can be explained as follows: when an Al foil is anodized into alumina, a volume expansion takes place [6]. Under a higher anodic voltage, the volume expansion increases and some cracks will appear in the alumina membrane. The formed alumina has a loose surface and is chemically unstable under open-circuit etching of the electrolyte. As a result, the solvent will continue to etch the alumina and therefore cause a nonlinear increase of $d_p$, as observed in our experiments.

The porosity $p$ of the PAA membrane can be calculated using an ideal geometrical structure model (hexagonal cell containing a central pore):

$$p = \frac{\pi}{2\sqrt{3}} \left(\frac{d_p}{d_c}\right)^2. \tag{2}$$

The dependence of the calculated porosity on the anodic voltage is displayed in Fig. 3. It is also not linear. The nonlinear increase of the porosity under high anodic voltage can similarly be explained according to the above discussion. Obviously, the change of nanopore geometrical structure under different anodic voltages will produce an influence on the anodic current. The average current density during the anodization of the second step vs the applied voltage is shown in the inset of Fig. 3. The curve is also nonlinear. A rapid increase of the current density with the applied voltage can clearly be observed. We know that the measured current density is a product of the porosity and the local current density at the electrolyte/alumina interface located at the bottom of each nanopore. High anodic voltage (high electrical field) can lead to both high local current density and large porosity. Therefore, the measured current density will drastically increase with the anodic voltage. This will largely affect the PL behavior of the PAA membrane, which will be discussed in the following.

From the above experimental results, we have seen that the anodic voltage directly determines the nanopore geomet-

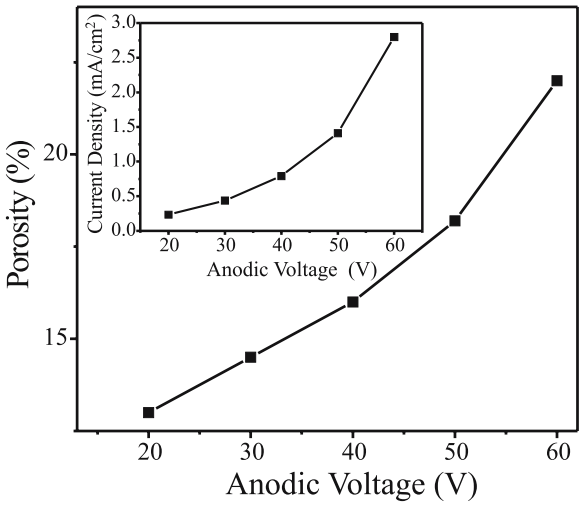


**FIGURE 3** Porosity as a function of the applied anodic voltage. The *inset* shows the dependence of the average current density during anodization of the second step on the applied anodic voltage

rical structure. Therefore, we can reveal the dependence of the blue PL band on the nanopore geometrical structure by investigating the PL peak position and intensity as a function of the anodic voltage. The PL spectra of the PAA membranes formed in 0.5 M oxalic acid under different anodic voltages are shown in Fig. 4, taken under excitation with the 300-nm line of a Xe lamp. All the membranes display an asymmetrical blue PL band whose peak position shows a red shift with increasing interpore distance/nanopore diameter. To identify the dependence of the blue PL band on the nanopore geometrical structure, similar to our previous work [20], the asymmetrical PL band was Gaussian divided into two subbands (dashed lines). The subband at the high-energy side (labeled as band 1) can be attributed to optical transitions in the $F^+$ centers (oxygen vacancy with only one electron), while the subband at the low-energy side (labeled as band 2) originates in the $F$ centers (oxygen vacancy with two electrons) [20]. These defect centers exist in pore walls and barrier layers of the PAA membrane. Table 1 summarizes some experimental parameters, including anodic voltage, pore diameter, interpore distance, porosity, and PL peak positions (i.e. emission energy). We can see that all the involved parameters monotonically increase with the anodic voltage. The two subbands have two sharp features. One is the change of their relative intensity with the applied voltage. This can be understood as follows: oxygen ions transform from $OH^-$ in the electrolyte and migrate through the barrier layer under a high electric field (about $10^{-7}$ V cm$^{-1}$) by a vacancy mechanism [25–27]. Therefore, the $F$ and $F^+$ centers are produced from partial oxygen vacancies remaining in the formed PAA membrane. The concentration of oxygen vacancies in the membrane is inversely proportional to that of $OH^-$ in the electrolyte. When the anodic process is conducted under a high applied voltage, the current density will greatly increase and thus the consumption of $OH^-$ will also increase. This will lead to the $OH^-$ concentration being lower in the electrolyte near the anode and therefore it is difficult for metallic Al to form stoichiometric alumina due to a temporary deficiency of $OH^-$ in the local electrolyte. As a result, a large amount of oxygen-deficient centers will be produced in the pore walls and barrier layers. Previous investigations of oxygen-deficient centers in crystalline alumina have shown that these defect centers have a complex structure and a conversion from the $F^+$ to $F$ centers may occur [28]:

$$F^+ + \mathrm{e} \rightarrow F, \tag{3}$$

where free electrons are from anions in the electrolyte (such as $OH^-$ and $O^{2-}$). If the $F^+$ centers are equally converted to the $F$ centers, more electrons are needed to meet the increase of the total amount of oxygen-deficient centers. However, the amount of free electrons in the electrolyte will reduce due to the decrease of the $OH^-$ concentration. Hence, this conversion only occurs to a certain extent because of the absence of electrons. This will cause the concentration of the $F^+$ centers relative to the $F$ centers to increase. Since the presence of the $F^+$ and $F$ centers in the PAA membrane is responsible for bands 1 and 2, respectively, the increase of the in-

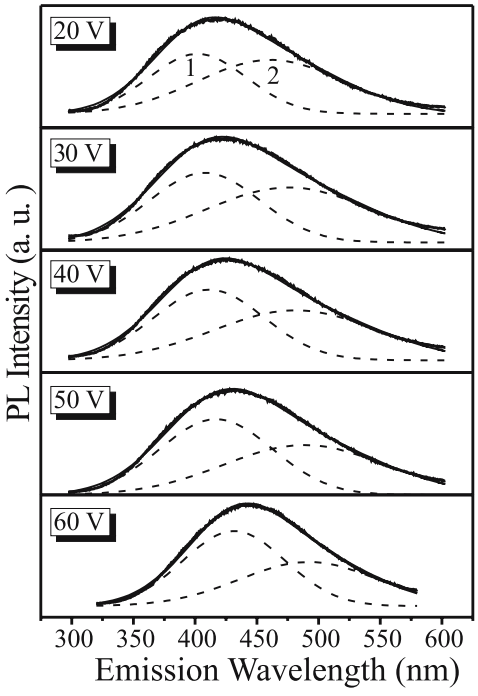


**FIGURE 4** PL spectra of the PAA membranes formed using anodization of Al foils in 0.5 M oxalic acid under different constant dc voltages of 20, 30, 40, 50, and 60 V, respectively. Each spectrum can be Gaussian divided into two subbands, which are shown in *dashed lines* and labeled as 1 and 2

| $U_a$ (V) | $d_p$ (nm) | $d_c$ (nm) | $p$ (%) | $\lambda$ (nm) | $\lambda_1$ (nm) | $\lambda_2$ (nm) |
|---|---|---|---|---|---|---|
| 20 | 22 | 58 | 13.0 | 421 | 409 | 460 |
| 30 | 32 | 80 | 14.5 | 426 | 414 | 472 |
| 40 | 43 | 100 | 16.0 | 429 | 417 | 477 |
| 50 | 56 | 125 | 18.2 | 434 | 422 | 483 |
| 60 | 72 | 146 | 22.0 | 443 | 432 | 492 |

**TABLE 1** Some geometrical structure parameters of the PAA membranes, including anodic voltage $U_a$, pore diameter $d_p$, interpore distance $d_c$, and porosity $p$. The peak positions, $\lambda$, $\lambda_1$, and $\lambda_2$ of the measured PL band, band 1, and band 2 are also presented for comparison

tensity of band 1 ($I1$) relative to that of band 2 ($I2$) reflects the change of relative concentration of the $F^+$ to the $F$ centers. Figure 5 shows the dependence of the ratio $I1/I2$ on the applied voltage. One can see that the ratio almost linearly increases with the applied anodic voltage. This draws us to infer that the relative concentration of the $F^+$ to the $F$ centers in the PAA membrane also linearly increases with the anodic voltage. The other feature of the two subbands is that their peak positions show a red shift on increasing the anodic voltage, as shown in the inset of Fig. 5. The red shift can be attributed to two factors, an accumulation of internal stress and an increase of oxygen-vacancy concentration in the PAA membrane [20, 29, 30]. We have previously elucidated that the concentration of oxygen-deficient centers increases with the current density (or anodic voltage). Meanwhile, remarkable internal stress will also accumulate in the PAA membrane due to the rapid growth rate [20]. The two factors make the energy levels of oxygen-deficient centers narrow [20, 29, 30]. Thus, the emission energies of the two subbands decrease. As a result, the two blue bands, which can be attributed to optical transitions between the energy levels in oxygen-deficient centers, show a red shift. It is worth noting that the red shift of band 2 is more obvious than that of band 1, which implies that the influence of the two above-mentioned factors on the $F$ centers is greater than that on the $F^+$ centers. This may be due to the difference in microstructure and level structure of the two defect centers.

The above analyses have revealed that the $F^+$ centers can be converted to the $F$ centers with supplied electrons. To further understand the conversion and its influence on the PL behavior, the PAA membrane formed under the anodic voltage of 40 V was irradiated by the 240-nm line of a Xe lamp. To obtain large irradiation power, the slit width was set at 10 mm, which will reduce the effect caused by the illumination of excitation light in considering the dependence of the PL intensities on UV irradiation time. Ultraviolet irradiation will cause similar conversion between oxygen-deficient centers [28]. We in situ measured the PL spectra under excitation with the 300-nm line of a Xe lamp and found that the peak positions

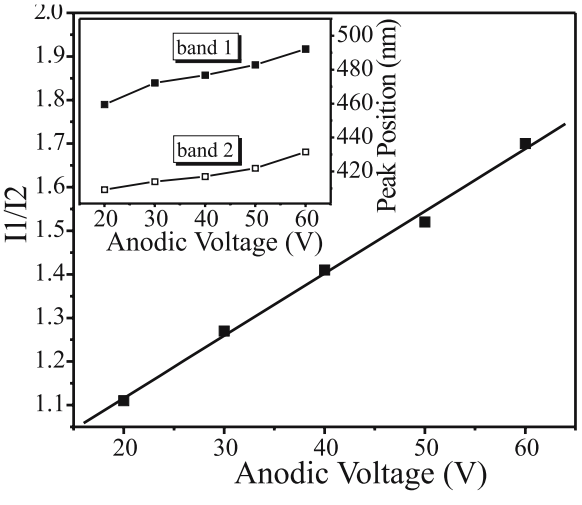


**FIGURE 5** The intensity ratio ($I1/I2$) of band 1 to band 2 as a function of the applied anodic voltage. The *inset* shows the peak positions of band 1 and band 2 vs the applied anodic voltage

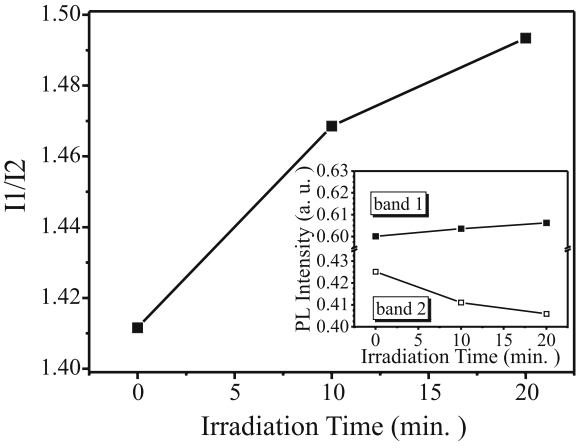


**FIGURE 6** The intensity ratio ($I1/I2$) of band 1 to band 2 as a function of ultraviolet irradiation time. The *inset* shows the PL intensities of bands 1 and 2 as a function of ultraviolet irradiation time

of the two subbands remain unchanged, but their relative intensity changes with irradiation time. Figure 6 shows the ratio $I1/I2$ as a function of ultraviolet irradiation time. The inset shows the dependence of the intensities of bands 1 and 2 on irradiation time. One can see that the intensity of band 1 slightly increases, but that of band 2 evidently decreases on increasing the irradiation time. The ratio $I1/I2$ increases by 5.7% after ultraviolet irradiation of 20 min. In previous studies of oxygen-deficient centers of crystalline alumina [28, 31], electrons in energy levels of the defect centers may be excited to the conduction band of the crystal or some other electrons can be trapped in defect levels of the band gap under ultraviolet irradiation. Thus, different defect centers will transform each other. This is similar to ultraviolet excitation in our experiments. For the PAA membranes with ultraviolet irradiation, the total effect of the conversion may be expressed as follows:

$$F + h\upsilon \rightarrow F^+ + \mathrm{e}, \tag{4}$$

$$F^+ + h\upsilon \rightarrow F^{2+} + \mathrm{e}. \tag{5}$$

The production (4) and annihilation (5) of the $F^+$ centers occur simultaneously and are nearly balanced; therefore, the concentration of the $F^+$ centers almost keeps unchanged. But, the $F$ centers are destroyed under ultraviolet irradiation. This makes the concentration of the $F$ centers obviously reduced. Correspondingly, the intensity ratio, $I1/I2$, increases as a function of ultraviolet irradiation time, as shown in Fig. 6.

We have investigated microstructural features and PL behavior of the PAA membranes formed using anodization of Al foils in 0.5 M oxalic acid under different dc voltages, and established a dependence of the observed blue PL peak position on the nanopore geometrical structure. We have Gaussian divided the asymmetrical blue PL band into two subbands, which originate in two kinds of oxygen-deficient centers, $F^+$ and $F$ centers, respectively. On raising the anodic voltage, the two subbands red shift and the intensity of the subband from the $F^+$ centers relative to that from the $F$ centers increases. This suggests that the increases of nanopore size and porosity under high anodic voltage make partial $F^+$ centers transform into the $F$ centers. We have discussed the conversion mechanism between the different defect centers on the basis of the PL

behavior of the PAA membrane under ultraviolet irradiation. This work will be beneficial to the better understanding of the PL property of the PAA membrane.

**ACKNOWLEDGEMENTS** This work was supported by Grant Nos. 10225416, 60466038, and 60421003 from the Natural Science Foundation of China and the LAPEM. Partial support was also from the Major State Basic Research Project No. G001CB3095 of China, Hong Kong Research Grants Council (RGC) Competitive Earmarked Research Grants (CERG) Nos. CityU 1137/03E and CityU 1120/04E, and City University of Hong Kong Strategic Research Grant (SRG) No. 7001642.

## REFERENCES

1 Y. Yamamoto, N. Baba, S. Tajima: Nature (Lond.) **289**, 572 (1981)
2 R.C. Furneaux, W.R. Rigby, A.P. Davidson: Nature **337**, 147 (1989)
3 H. Masuda, K. Fukuda: Science **268**, 1466 (1995)
4 H. Masuda, H. Yamada, M. Satoh, H. Asoh, M. Nakao, T. Tamamura: Appl. Phys. Lett. **71**, 2770 (1997)
5 A.P. Li, F. Müller, A. Birner, K. Nielsch, U. Gösele: J. Appl. Phys. **84**, 6023 (1998)
6 O. Jessensky, F. Müller, U. Gösele: Appl. Phys. Lett. **72**, 1173 (1998)
7 L. Pu, X.M. Bao, J.P. Zou, D. Feng: Angew. Chem. **113**, 1538 (2001)
8 M.S. Sander, L.S. Tan: Adv. Funct. Mater. **13**, 393 (2003)
9 K.L. Hobbs, P.R. Larson, G.D. Lian, J.C. Keay, M.B. Johnson: Nano Lett. **4**, 167 (2004)
10 J. Li, C. Papadopoulos, J.M. Xu: Nature **402**, 253 (1999)
11 J.C. Bao, C.Y. Tie, Z. Xu, Q.F. Zhou, D. Shen, Q. Ma: Adv. Mater. **13**, 1631 (2001)
12 S.H. Jeong, Y.K. Cha, I.K. Yoo, Y.S. Song, C.W. Chung: Chem. Mater. **16**, 1612 (2004)
13 P. Hoyer, N. Baba, H. Masuda: Appl. Phys. Lett. **66**, 2700 (1995)
14 Y. Li, G.W. Meng, L.D. Zhang, F. Phillipp: Appl. Phys. Lett. **76**, 2011 (2000)
15 G.S. Wu, L.D. Zhang, B.C. Cheng, T. Xie, X.Y. Yuan: J. Am. Chem. Soc. **126**, 5976 (2004)
16 Y. Du, W.L. Cai, C.M. Mo, J. Chen, L.D. Zhang, X.G. Zhu: Appl. Phys. Lett. **74**, 2951 (1999)
17 Y. Li, G.H. Li, G.W. Meng, L.D. Zhang, F. Phillipp: J. Phys.: Condens. Matter **13**, 2691 (2001)
18 T. Gao, G.W. Meng, L.D. Zhang: J. Phys.: Condens. Matter **15**, 2071 (2003)
19 G.H. Li, Y. Zhang, Y.C. Wu, L.D. Zhang: J. Phys.: Condens. Matter **15**, 8663 (2003)
20 G.S. Huang, X.L. Wu, Y.F. Mei, X.F. Shao, G.G. Siu: J. Appl. Phys. **93**, 582 (2003)
21 H. Masuda, M. Satoh: Jpn. J. Appl. Phys. Part 2 **35**, 126 (1996)
22 S. Shingubara, O. Okino, Y. Sayama, H. Sakaue, T. Takahagi: Jpn. J. Appl. Phys. Part 1 **36**, 7791 (1997)
23 F. Keller, M.S. Hunter, D.L. Robinson: J. Electrochem. Soc. **100**, 411 (1953)
24 V.P. Parkhutik, V.I. Shershulsky: J. Phys. D: Appl. Phys. **25**, 1258 (1992)
25 J.W. Diggle, T.C. Downie, C.W. Goulding: Chem. Rev. (Washington, DC) **69**, 365 (1969)
26 C. Cherki, J. Siejka: J. Electrochem. Soc. **120**, 784 (1973)
27 J. Siejka, C. Ortega: J. Electrochem. Soc. **124**, 883 (1977)
28 G.J. Pogatshnik, Y. Chen, B.D. Evans: IEEE Trans. Nucl. Sci. **34**, 1709 (1987)
29 J.K. Vassiliou, V. Mehrotra, M.W. Russell, E.P. Giannelis, R.D. McMichael, R.D. Shull, R.F. Ziolo: J. Appl. Phys. **73**, 5109 (1993)
30 H.R. Phillipp: J. Phys. Chem. Solids **32**, 1935 (1971)
31 G.H. Rosenblatt, M.W. Rowe, G.P. Williams, R.T. Williams, Y. Chen: Phys. Rev. B **39**, 10 309 (1989)